

Fourier Analysis-based Iterative Combinatorial Auctions

Jakob Weissteiner^{1*} Chris Wendler^{2*} Sven Seuken¹ Ben Lubin³ Markus Püschel²

¹UNIVERSITY OF ZÜRICH

Department of Informatics

²ETH ZÜRICH

Department of Informatics

³BOSTON UNIVERSITY

Department of Information Systems

weissteiner@ifi.uzh.ch, chris.wendler@inf.ethz.ch, seuken@ifi.uzh.ch, blubin@bu.edu, pueschel@inf.ethz.ch

Abstract

Recent advances in Fourier analysis have brought new tools to efficiently represent and learn set functions. In this paper, we bring the power of Fourier analysis to the design of combinatorial auctions (CAs). The key idea is to approximate bidders' value functions using Fourier-sparse set functions, which can be computed using a relatively small number of queries. Since this number is still too large for real-world CAs, we propose a new hybrid design: we first use neural networks to learn bidders' values and then apply Fourier analysis to the learned representations. On a technical level, we formulate a Fourier transform-based winner determination problem and derive its mixed integer program formulation. Based on this, we devise an iterative CA that asks Fourier-based queries. We experimentally show that our hybrid ICA achieves higher efficiency than prior auction designs, leads to a fairer distribution of social welfare, and significantly reduces runtime. With this paper, we are the first to leverage Fourier analysis in CA design and lay the foundation for future work in this area.

1 Introduction

Combinatorial auctions (CAs) are used to allocate multiple heterogeneous items to bidders. CAs are particularly useful in domains where bidders' preferences exhibit *complementarities* and *substitutabilities* as they allow bidders to submit bids on *bundles* of items rather than on individual items.

Since the bundle space grows exponentially in the number of items, it is impossible for bidders to report values for all bundles in settings with more than a modest number of items. Thus, parsimonious preference elicitation is essential for the practical design of CAs. For general value functions, Nisan and Segal (2006) have shown that to achieve full efficiency in CAs, exponential communication in the number of items is needed in the worst case. Thus, practical CA designs cannot provide efficiency guarantees in large domains. Instead, recent proposals have focused on *iterative combinatorial auctions* (ICAs), where the auctioneer interacts with bidders over multiple rounds, eliciting a *limited* amount of information, aiming to find a highly efficient allocation.

ICAs have found widespread application in practice; most recently, for the sale of licenses to build offshore wind farms (Ausubel and Cramton 2011). For the sale of spectrum licenses, the combinatorial clock auction (CCA) (Ausubel, Cramton, and Milgrom 2006) has already generated more than \$20 billion in total revenue (Ausubel and Baranov 2017). Therefore, increasing the efficiency of such real-world ICAs by only 1–2% points translates into monetary gains of millions of dollars.

1.1 Machine Learning-based Auction Design

Recently, researchers have successfully used machine learning (ML) to improve the performance of CAs. Early work by Blum et al. (2004) and Lahaie and Parkes (2004) laid the foundation for this by studying the relationship between computational learning theory and preference elicitation in CAs. Dütting et al. (2019) and Rahme et al. (2020) used neural networks (NNs) to learn auction mechanisms from data, following the automated mechanism design paradigm. Brero, Lahaie, and Seuken (2019) introduced a Bayesian ICA using probabilistic price updates to achieve faster convergence. Most related to the present paper is the work by Brero, Lubin, and Seuken (2018; 2021), who developed a value-query-based ML-powered ICA using support vector regressions (SVRs) that achieves even higher efficiency than the CCA. In follow-up work, Weissteiner and Seuken (2020) extended their mechanism to NNs, further increasing the efficiency. However, especially in large domains, it remains a challenge to find the efficient allocation while keeping the elicitation cost for bidders low. Therefore, even state-of-the-art approaches suffer from significant efficiency losses and often result in unfair allocations, highlighting the need for better preference elicitation algorithms.

1.2 Combining Fourier Analysis and CAs

The goal of preference elicitation in CAs is to learn bidders' value functions using a small number of queries. Mathematically, value functions are *set functions*, which are in general exponentially large objects that are notoriously hard to represent or learn. To control for this complexity, we leverage Fourier analysis for set functions (Bernasconi, Codenotti, and Simon 1996; O'Donnell 2014; Püschel and Wendler

*These authors contributed equally.

2020). In particular, we consider *Fourier-sparse approximations*, which are represented by a small number of parameters. These parameters are the non-zero Fourier coefficients (FCs) obtained by a base change with the Fourier transform (FT). We use the framework by Püschel and Wendler (2020), which contains new FTs beyond the classical Walsh-Hadamard transform (WHT) (Bernasconi, Codenotti, and Simon 1996), providing additional flexibility.

Until recently, methods for learning Fourier-sparse set functions focused only on the WHT, and they placed assumptions on bidders' value functions that are too restrictive for CAs (Stobbe and Krause 2012). However, recently, Amrollahi et al. (2019) proposed a new algorithm that can approximate general set functions by WHT-sparse ones, which is suitable for large CAs and we use it in this work.

1.3 Our Contribution

Our main contribution in this paper is to bring the power of Fourier analysis to CA design (Section 3). In particular, we formulate *FT-based winner determination problems (WDPs)* and derive corresponding mixed integer programs (MIPs) for several notions of FTs (Section 4). Our MIPs allow for the efficient solution of the FT-based WDP. Thus, they provide the foundation for using Fourier-sparse approximations in auction design.

We first experimentally show that the WHT performs best among the FTs in terms of induced level of sparsity (Section 5.1) and reconstruction error (Section 5.2). As an initial approach to leveraging the WHT, we develop a WHT-based allocation rule (Section 5.3). However, this requires too many queries for direct use in CAs. To overcome this issue, we propose a practical hybrid ICA mechanism based on NNs and Fourier analysis (Section 6.1). The key idea is to compute Fourier-sparse approximations of NN-based bidder representations, enabling us to keep the number of queries small. The advantage of the NN-based representations is that they capture important aspects of the bidders' value functions (Section 6.2) and can be queried arbitrarily often.

Our efficiency experiments show that hybrid ICA achieves higher economic efficiency than state-of-the-art mechanisms, leads to a significant computational speedup, and yields fairer allocations (Section 6.3). Overall, our results show that leveraging Fourier analysis in CA design is a promising new research direction.

2 Preliminaries

In this section, we present our formal model and review the ML-based ICA by Brero, Lubin, and Seuken (2021).

2.1 Formal Model for ICAs

We consider a CA with n bidders and m indivisible items. Let $N = \{1, \dots, n\}$ and $M = \{1, \dots, m\}$ denote the set of bidders and items, respectively. We denote with $x \in \mathcal{X} = \{0, 1\}^m$ a bundle of items represented as an indicator vector, where $x_j = 1$ iff item $j \in M$ is contained in x . Bidders' true preferences over bundles are represented by their (private)

value functions $v_i : \mathcal{X} \rightarrow \mathbb{R}_+$, $i \in N$, i.e., $v_i(x)$ represents bidder i 's true value for bundle x .

By $a = (a_1, \dots, a_n) \in \mathcal{X}^n$ we denote an allocation of bundles to bidders, where a_i is the bundle bidder i obtains. We denote the set of *feasible* allocations by $\mathcal{F} = \{a \in \mathcal{X}^n : \sum_{i \in N} a_{ij} \leq 1, \forall j \in M\}$. The (true) *social welfare* of an allocation a is defined as $V(a) = \sum_{i \in N} v_i(a_i)$. We let $a^* \in \arg\max_{a \in \mathcal{F}} V(a)$ be a social-welfare maximizing, i.e., *efficient*, allocation. The efficiency of any $a \in \mathcal{F}$ is measured in terms of a^* by $V(a)/V(a^*)$.

An ICA *mechanism* defines how the bidders interact with the auctioneer and how the final allocation and payments are determined. We denote a bidder's (possibly untruthful) reported value function by $\hat{v}_i : \mathcal{X} \rightarrow \mathbb{R}_+$. In this paper, we consider ICAs that ask bidders to iteratively report their values $\hat{v}_i(x)$ for particular bundles x selected by the mechanism. A finite set of such reported bundle-value pairs of bidder i is denoted as $R_i = \{(x^{(l)}, \hat{v}_i(x^{(l)}))\}$, $x^{(l)} \in \mathcal{X}$. Let $R = (R_1, \dots, R_n)$ denote the tuple of reported bundle-value pairs obtained from all bidders and $R_{-i} = (R_1, \dots, R_{i-1}, R_{i+1}, \dots, R_n)$. We define the *reported social welfare* of an allocation a given R as $\hat{V}(a|R) = \sum_{i \in N: (a_i, \hat{v}_i(a_i)) \in R_i} \hat{v}_i(a_i)$, where $(a_i, \hat{v}_i(a_i)) \in R_i$ ensures that only values for reported bundles contribute. Finally, the optimal allocation $a_R^* \in \mathcal{F}$ given the reports R is defined as

$$a_R^* \in \arg\max_{a \in \mathcal{F}} \hat{V}(a|R). \quad (1)$$

The final allocation $a_R^* \in \mathcal{F}$ and payments $p \in \mathbb{R}_+^n$ are computed based on the elicited reports R only. We assume that bidders' utilities are of the form $u_i(a, p) = v_i(a_i) - p_i$.

As the auctioneer can generally only ask each bidder i for a limited number of bundle-value pairs $|R_i| \leq \kappa$ (e.g., $\kappa = 500$), the mechanism needs a sophisticated preference elicitation algorithm, with the goal of finding a highly efficient allocation a_R^* with a limited number of value queries.

2.2 A Machine Learning powered ICA

We now review the *machine learning-powered combinatorial auction (MLCA)* introduced by Brero, Lubin, and Seuken (2021). Instead of using SVRs as the ML algorithm, we describe MLCA using NNs \mathcal{N}_i (a variation introduced by Weissteiner and Seuken (2020)).

At the core of MLCA is a *query module* (Algorithm 1), which, for each bidder $i \in I$, determines a new value query

Algorithm 1: NN-QUERY MODULE (Brero et al. 2021)

Function : *NextQueries*(I, R)
Inputs : Index set of bidders I and reported values R
Parameters: Neural networks $\mathcal{N}_i : \mathcal{X} \rightarrow \mathbb{R}_+$, $i \in N$
1 **foreach** $i \in I$ **do** Fit \mathcal{N}_i on $R_i : \mathcal{N}_i[R_i] \triangleright$ *Estimation step*
2 Solve $q \in \arg\max_{a \in \mathcal{F}} \sum_{i \in I} \mathcal{N}_i[R_i](a_i) \triangleright$ *Optimization step*
3 **foreach** $i \in I$ **do**
4 **if** $q_i \in R_i$ **then** \triangleright *Bundle already queried*
5 Define $\mathcal{F}' = \{a \in \mathcal{F} : a_i \neq x, \forall x \in R_i\}$
6 Re-solve $q' \in \arg\max_{a \in \mathcal{F}'} \sum_{l \in I} \mathcal{N}_l[R_l](a_l)$
7 Update $q_i = q'_i$
8 **return** *profile of new queries* $q = (q_1, \dots, q_n)$

Algorithm 2: MLCA (Brero et al. 2021)

Params: $t = 1, Q^{\text{init}}, Q^{\text{max}}$ init. and max #queries per bidder

```
1 foreach  $i \in N$  do
2   | Receive reports  $R_i$  for  $Q^{\text{init}}$  randomly drawn bundles
3 while  $t \leq \lfloor (Q^{\text{max}} - Q^{\text{init}})/n \rfloor$  do ▷ Round iterator
4   |  $q^{\text{new}} = \text{NextQueries}(N, R)$  ▷ Main economy queries
5   | foreach bidder  $i \in N$  do ▷ Marginal economy queries
6     |  $q^{\text{new}} = q^{\text{new}} \cup \text{NextQueries}(N \setminus \{i\}, R_{-i})$ 
7   | foreach bidder  $i \in N$  do
8     | Receive reports  $R_i^{\text{new}}$  for  $q_i^{\text{new}}$ , set  $R_i = R_i \cup R_i^{\text{new}}$ 
9   |  $t = t + 1$ 
10 From reports  $R$  compute  $a_R^*$  as in (1) and VCG payments  $p$ 
11 return final allocation  $a_R^*$  and payments  $p$ 
```

q_i . First, in the *estimation step* (Line 1), NNs are used to learn bidders' valuations from reports R_i . Next, in the *optimization step* (Line 2), a NN-based WDP is solved to find a candidate q of value queries. See Weissteiner and Seuken (2020) for details on the NN-based *estimation* and *optimization step*. Finally, if q_i has already been queried before (Line 4), another, more restricted NN-based WDP (Line 6) is solved and q_i is updated correspondingly. This ensures that all final queries q are new.

In Algorithm 2, we present MLCA in a slightly abbreviated form. MLCA proceeds in rounds until a maximum number of queries per bidder Q^{max} is reached. In each round, it calls Algorithm 1 $n + 1$ times: once including all bidders (Line 4, *main economy*) and n times excluding one bidder (Lines 5–6, *marginal economies*). At the end of each round, the mechanism receives reports R^{new} from all bidders for the newly generated queries q^{new} , and updates the overall elicited reports R (Lines 7–8). In Line 10, MLCA computes an allocation a_R^* that maximizes the reported social welfare and determines VCG payments p (see Appendix A.1).

2.3 Incentives of MLCA and Hybrid ICA

In CA design, we care not only about the preference elicitation process, but also about bidders' incentives. A CA with bad incentives leads to misreports, which can significantly hurt efficiency. MLCA is not strategyproof, like all deployed spectrum auctions (including the CCA (Ausubel and Baranov 2017)). However, Brero, Lubin, and Seuken (2021) argue that it has good incentives in practice. We briefly review their key arguments.

First, when using VCG, bidder i 's utility is:

$$u_i = v_i((a_R^*)_i) + \underbrace{\sum_{j \in N \setminus \{i\}} \hat{v}_j((a_R^*)_j)}_{\text{(a) Reported SW of main economy}} - \underbrace{\sum_{j \in N \setminus \{i\}} \hat{v}_j((a_{R_{-i}}^*)_j)}_{\text{(b) Reported SW of marginal economy}}.$$

Any beneficial misreport must increase (a) – (b).

MLCA has two features that mitigate manipulations. First, MLCA explicitly queries each bidder's marginal economy (Algorithm 2, Line 5), which implies that (b) is practically independent of bidder i 's bid (Brero, Lubin, and Seuken (2021) provide experimental support for this). Second, MLCA enables bidders to “push” information to the auction which they deem useful. This mitigates certain manipulations that target (a), as it allows bidders to increase (a)

with truthful information. Brero, Lubin, and Seuken (2021) argue that any remaining manipulation would be implausible as it would require almost complete information.

If we are willing to make two weak assumptions, we also obtain a theoretical incentive guarantee. Assumption 1 requires that, if all bidders bid truthfully, then MLCA finds an efficient allocation (we show in Section 6.3 that in two of our domains, we indeed find the efficient allocation in the majority of cases). Assumption 2 requires that, for all bidders i , if all other bidders report truthfully, then the social welfare of bidder i 's marginal economy is independent of his value reports. If both assumptions hold, then bidding truthfully is an ex-post Nash equilibrium in MLCA.

In Section 6.1, we present our *hybrid ICA*, which only differs from MLCA in how the queries are generated. Thus, the incentive analysis for MLCA extends to our *hybrid ICA*.

3 Fourier Analysis of Value Functions

In this section, we show how to apply Fourier analysis to bidders' value functions and provide the theoretical foundation of Fourier transform-based WDPs.

Classic Fourier analysis decomposes an audio signal or image into an orthogonal set of sinusoids of different frequencies. Similarly, the classical Fourier analysis for *set functions* (i.e., functions mapping each subset of a discrete set to a scalar) decomposes a set function into an orthogonal set of Walsh functions (Bernasconi, Codenotti, and Simon 1996), which are piecewise constant with values 1 and -1 only. Recent work by Püschel and Wendler (2020) extends the Fourier analysis for set functions with several novel forms of set Fourier transforms (FTs). Importantly, because bidders' value functions are set functions, they are amenable to this type of Fourier analysis, and it is this connection that we will leverage in our auction design.

Sparsity. The motivation behind our approach is that we expect bidders' value functions to be *sparse*, meaning that their preferences can be described with much less data than is contained in the (exponentially-sized) full value function. While this sparsity may be difficult to uncover when looking at bidders' value reports, it may reveal itself in the Fourier domain (where then most Fourier coefficients (FCs) are zero). As all FTs are changes of basis, each FT provides us with a new *lens on the bidder's value function*, potentially revealing structure and thus reducing dimensionality.

Set function Fourier transform. We now provide a formal description of FTs for reported value functions \hat{v}_i . To do so, we represent \hat{v}_i as a vector $(\hat{v}_i(x))_{x \in \mathcal{X}}$. Each known FT is a change of basis and thus can be represented by a certain matrix $F \in \{-1, 0, 1\}^{2^m \times 2^m}$ with the form:

$$\phi_{\hat{v}_i}(y) = (F\hat{v}_i)(y) = \sum_{x \in \mathcal{X}} F_{y,x} \hat{v}_i(x). \quad (2)$$

The corresponding inverse transform F^{-1} is thus:

$$\hat{v}_i(x) = (F^{-1}\phi_{\hat{v}_i})(x) = \sum_{y \in \mathcal{Y}} F_{x,y}^{-1} \phi_{\hat{v}_i}(y). \quad (3)$$

$\phi_{\hat{v}_i}$ is again a set function and we call $\phi_{\hat{v}_i}(y)$ the *Fourier coefficient* at frequency y . A value function is *Fourier-sparse*

if $|\text{supp}(\phi_{\tilde{v}_i})| = |\{y : \phi_{\tilde{v}_i}(y) \neq 0\}| \ll 2^m$. We call $\text{supp}(\phi_{\tilde{v}_i})$ the *Fourier support* of \tilde{v}_i .

Classically, the WHT is used as F (Bernasconi, Codenotti, and Simon 1996; O'Donnell 2014), but we also consider two recently introduced FTs (FT3, FT4) due to their information-theoretic interpretation given in Püschel and Wendler (2020):

$$\text{FT3: } F_{y,x} = (-1)^{|y|-|x|} \mathbb{I}_{\min(x,y)=x}, \quad (4)$$

$$\text{FT4: } F_{y,x} = (-1)^{|\min(x,y)|} \mathbb{I}_{\max(x,y)=1_m}, \quad (5)$$

$$\text{WHT: } F_{y,x} = \frac{1}{2^m} (-1)^{|\min(x,y)|}. \quad (6)$$

Here, \min is the elementwise minimum (intersection of sets), \max analogously, $|\cdot|$ is the set size, 1_m denotes the m -dimensional vector of 1s, and the indicator function \mathbb{I}_P is equal to 1 if the predicate P is true and 0 otherwise.

Fact 1. Note that the FT3 is identical to the classical polynomial value function representation (Lahaie 2010a,b) $\hat{v}_i^{\text{poly}} : \mathcal{X} \mapsto \mathbb{R}_+$ defined as

$$\hat{v}_i^{\text{poly}}(x) = \sum_{l=1}^m \sum_{j=\{j_1, \dots, j_l\} \subseteq M} x_{j_1} \cdot \dots \cdot x_{j_l} \cdot c_j^{(i)}. \quad (7)$$

where the coefficient $c_j^{(i)}$ is equal to the FT3 FC at frequency y with $y_i = 1$ for $i \in \{j_1, \dots, j_l\}$ and $y_i = 0$ else. This can be seen by calculating the inverse in (4), i.e., $F_{y,x}^{-1} = \mathbb{I}_{\min(x,y)=x}$, and plugin $F_{y,x}^{-1}$ into (3). E.g. for two items $M = \{1, 2\}$, $\hat{v}_i^{\text{poly}}(x) = x_1 c_{\{1\}}^{(i)} + x_2 c_{\{2\}}^{(i)} + x_1 x_2 c_{\{1,2\}}^{(i)}$.

Notions of Fourier-sparsity. In recent years, the notion of Fourier-sparsity has gained considerable attention, leading to highly efficient algorithms to compute FTs (Stobbe and Krause 2012; Amrollahi et al. 2019; Wendler et al. 2020). Many classes of set functions are Fourier-sparse (e.g., graph cuts, hypergraph valuations and decision trees (Abraham et al. 2012)) and can thus be learned efficiently. The benefit of considering multiple FTs is that they offer different, non-equivalent notions of sparsity (see Appendix B).

Fourier-sparse approximations. In practice, \hat{v}_i may only be approximately sparse. Meaning that while not being sparse, it can be approximated well by a Fourier-sparse function \tilde{v}_i . Formally, let $\mathcal{S}_i = \text{supp}(\phi_{\tilde{v}_i})$ with $|\mathcal{S}_i| = k$, we call

$$\tilde{v}_i(x) = \sum_{y \in \mathcal{S}_i} F_{x,y}^{-1} \phi_{\tilde{v}_i}(y) \text{ for all } x \in \mathcal{X} \quad (8)$$

a k -Fourier-sparse approximation of \hat{v}_i if $\|\hat{v}_i - \tilde{v}_i\|_2^2$ is small. We denote the vector of FCs by $\phi_{\tilde{v}_i|_{\mathcal{S}_i}} = (\phi_{\tilde{v}_i}(y))_{y \in \mathcal{S}_i}$.

4 Fourier Transform-based WDPs

To leverage Fourier analysis for auction design, we represent bidders' reported value functions using Fourier-sparse approximations. An important step in most auction designs is to find the social welfare-maximizing allocation given bidder's reports, which is known as the *Winner Determination Problem* (WDP). Thus, to apply FTs in such mechanisms, we need to be able to solve the WDP efficiently. Accordingly, we next derive MIP formulations for each of the FTs.

For each bidder $i \in N$, let $\tilde{v}_i : \mathcal{X} \rightarrow \mathbb{R}_+$ be the Fourier-sparse approximation of the bidders' reported value function \hat{v}_i . Next, we define the *Fourier transform-based WDP*.

Definition 1. (FOURIER TRANSFORM-BASED WDP)

$$\text{argmax}_{a \in \mathcal{F}} \sum_{i \in N} \tilde{v}_i(a_i). \quad (\text{FT-WDP})$$

For all $x, y \in \mathbb{R}^d$, let $x \leq y$, $\max(x, y)$ and $(-1)^x$ be defined component-wise, and let $\langle \cdot, \cdot \rangle$ denote the Euclidean scalar product. First, we formulate succinct representations of \tilde{v}_i for all considered FTs.

Lemma 1. (SUCCINCT REPRESENTATIONS) For $i \in N$ let $\mathcal{S}_i = \{y^{(1)}, \dots, y^{(k)}\}$ be the support of a k -Fourier-sparse approximation \tilde{v}_i and $W_i \in \{0, 1\}^{k \times m}$ be defined as $(W_i)_{l,j} = \mathbb{I}_{y_j^{(l)}=1}$. Then \tilde{v}_i can be rewritten as:

$$\text{FT3: } \tilde{v}_i(x) = \langle \phi_{\tilde{v}_i|_{\mathcal{S}_i}}, \max(0_k, 1_k - W_i(1_m - x)) \rangle \quad (9)$$

$$\text{FT4: } \tilde{v}_i(x) = \langle \phi_{\tilde{v}_i|_{\mathcal{S}_i}}, \max(0_k, 1_k - W_i x) \rangle \quad (10)$$

$$\text{WHT: } \tilde{v}_i(x) = \langle \phi_{\tilde{v}_i|_{\mathcal{S}_i}}, (-1)^{W_i x} \rangle. \quad (11)$$

Please see Appendix C.1 for the proof. Using Lemma 1 and rewriting $\max(\cdot, \cdot)$ and $(-1)^{\cdot}$ as linear constraints, we can formulate (FT-WDP) as a MIP.

Theorem 1. (FOURIER TRANSFORM-BASED MIPS) Let $\tilde{v}_i : \mathcal{X} \rightarrow \mathbb{R}$ be a k -Fourier-sparse approximation as defined in (9), (10), or (11). Then there exists a constant $C > 0$ such that the MIP defined by the following objective

$$\text{argmax}_{a \in \mathcal{F}, \beta_i \in \{0,1\}^k} \sum_{i \in N} \langle \phi_{\tilde{v}_i|_{\mathcal{S}_i}}, \alpha_i \rangle, \quad (12)$$

and for $i \in N$ one set of transform specific constraints (13)–(15), or (16)–(18), or (19)–(21), is equivalent to (FT-WDP).

$$\text{FT3: } \text{s.t. } \alpha_i \geq 1_k - W_i(1_m - a_i) \quad (13)$$

$$\alpha_i \leq 1_k - W_i(1_m - a_i) + C\beta_i \quad (14)$$

$$0_k \leq \alpha_i \leq C(1_k - \beta_i) \quad (15)$$

$$\text{FT4: } \text{s.t. } \alpha_i \geq 1_k - W_i a_i \quad (16)$$

$$\alpha_i \leq 1_k - W_i a_i + C\beta_i \quad (17)$$

$$0_k \leq \alpha_i \leq C(1_k - \beta_i) \quad (18)$$

$$\text{WHT: } \text{s.t. } \alpha_i = -2\beta_i + 1_k \quad (19)$$

$$\beta_i = W_i a_i - 2\gamma_i \quad (20)$$

$$\gamma_i \in \mathbb{Z}^k \quad (21)$$

See Appendix C.2 for the proof. Using Theorem 1, we can solve (FT-WDP) using standard MIP solvers like CPLEX.

5 Analyzing the Potential of a FT-based CA

In this section, we experimentally evaluate the FTs and propose an FT-based allocation rule that motivates our practical hybrid ICA mechanism presented later in Section 6.

For our experiments, we use the spectrum auction test suite (SATS) version 0.6.4 (Weiss, Lubin, and Seuken 2017). SATS enables us to generate synthetic CA instances in different domains. We have access to each bidder's *true* full

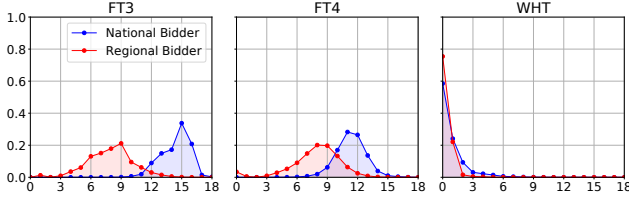


Figure 1: Spectral energy distribution in LSVM for different notions of FTs. For each cardinality (x-axis), we collect the spectral energy (y-axis) of all frequencies of that cardinality and normalize by the total spectral energy.

value function v_i and the efficient allocation a^* . When simulating bidders, we assume truthful bidding (i.e., $\hat{v}_i = v_i$). We consider three domains:

The Global Synergy Value Model (GSVM) (Goeree and Holt 2010) has 18 items, 6 *regional* and 1 *national bidder*.

The Local Synergy Value Model (LSVM) (Scheffel, Ziegler, and Bichler 2012) consists of 18 items, 5 *regional* and 1 *national bidder*. Complementarities arise from spatial proximity of items.

The Multi-Region Value Model (MRVM) (Weiss, Lubin, and Seuken 2017) has 98 items and 10 bidders (categorized as *local*, *regional*, or *national*) and models large US spectrum auctions.

5.1 Notions of Fourier Sparsity

We first experimentally show that different notions of FT lead to different types of sparsity in LSVM (for GSVM and MRVM see Appendix D.1). In order to do so, we first compute the FTs of all bidders and then calculate their corresponding *spectral energy* distribution. That is, for each cardinality (i.e., number of items) d from 0 to m , we compute $\sum_{y \in \mathcal{X}: |y|=d} \phi_{\hat{v}_i}(y)^2 / \sum_{y \in \mathcal{X}} \phi_{\hat{v}_i}(y)^2$. In Figure 1 we present the mean over 30 LSVM instances and bidder types.

Figure 1, shows that while the energy is spread among FCs of various degrees in FT3 and FT4, in WHT the low degree (≤ 2) FCs contain most of the energy, i.e., the WHT has much fewer important FCs that accurately describe each bidder’s value function. Moreover, as the WHT is orthogonal, we can conclude that learning low degree WHT-sparse approximations, leads to low reconstruction error in LSVM. Low degree WHT-sparse approximations can be learnt efficiently and accurately from a small number of queries using the compressive sensing method (Stobbe and Krause 2012).

Recall, that FT3 is identical to the classical polynomial value function representation \hat{v}_i^{poly} from (7). Thus, we see that converting the classical polynomial representation into another FT basis (here WHT) can indeed be very helpful for the design of ML-based CAs.

5.2 Reconstruction Error of Fourier Transforms

Next we validate the FT approach by comparing the reconstruction error of the FTs in the medium-sized GSVM and LSVM, where we can still compute the full FT (in contrast to MRVM). For now, we assume that we have access to

| DOMAIN | K | BIDDER | FT3 | FT4 | WHT | NN |
|--------|-----|--------|----------------|------------------|----------------|----------------|
| GSVM | 100 | NAT. | 11.3 \pm 0.7 | 14.2 \pm 0.8 | 1.8 \pm 0.1 | 9.0 \pm 1.8 |
| | | REG. | 0.0 \pm 0.0 | 1.4 \pm 0.2 | 0.4 \pm 0.1 | 7.2 \pm 0.9 |
| | 200 | NAT. | 0.0 \pm 0.0 | 0.0 \pm 0.0 | 0.0 \pm 0.0 | 5.7 \pm 0.4 |
| | | REG. | 0.0 \pm 0.0 | 0.0 \pm 0.0 | 0.0 \pm 0.0 | 5.2 \pm 0.8 |
| LSVM | 100 | NAT. | 78.4 \pm 1.0 | 580.2 \pm 7.9 | 31.2 \pm 0.4 | 48.7 \pm 1.2 |
| | | REG. | 28.2 \pm 2.3 | 48.5 \pm 2.7 | 6.8 \pm 0.3 | 17.8 \pm 0.7 |
| | 200 | NAT. | 95.8 \pm 1.2 | 639.0 \pm 10.0 | 26.2 \pm 0.3 | 40.6 \pm 0.7 |
| | | REG. | 25.8 \pm 2.0 | 43.1 \pm 2.4 | 5.3 \pm 0.3 | 15.3 \pm 0.9 |

Table 1: Reconstruction error with a 95%-CI of k -Fourier sparse approximations \tilde{v}_i and NNs trained on k randomly selected bundles. Winners are marked in grey.²

bidders’ full \hat{v}_i . In Procedure 1, we determine the best k -Fourier-sparse approximation \tilde{v}_i (see Appendix D.2)

Procedure 1. (BEST FCs GIVEN FULL ACCESS TO \hat{v}_i)
Compute the k best FCs $\phi_{\hat{v}_i|S_i}$ in terms of L2 error by using the full FT for each bidders’ reported value function $\phi_{\hat{v}_i} = F\hat{v}_i$.

Using \hat{v}_i , we then calculate the reconstruction RMSE $(\frac{1}{2^m} \sum_{x \in \mathcal{X}} (\hat{v}_i(x) - \tilde{v}_i(x))^2)^{1/2}$ averaged over 100 instances and bidders of the same type. In Table 1, we present the RMSEs for the three FTs and for NNs, where we used the same architectures as in Weissteiner and Seuken (2020).

For GSVM, we observe that we can perfectly reconstruct \hat{v}_i with the 200 best FCs, which shows that GSVM is 200-sparse. In contrast, LSVM is non-sparse, and we do not achieve perfect reconstruction with 200 FCs. Overall, we observe that the WHT outperforms FT3 and FT4. Moreover, we see that, if we could compute the k best FCs of the WHT from k training points, the WHT would outperform the NNs. However, in practice, we do not have access to full value functions. Instead, we must use an algorithm that computes the best FCs using a reasonable number of value queries.

5.3 A Fourier Transform-based Allocation Rule

We now present an FT-based allocation rule using the *robust sparse WHT algorithm (RWHT)* by Amrollahi et al. (2019). RWHT learns a Fourier-sparse approximation \tilde{v}_i of \hat{v}_i from queries. We use Procedure 2 to find the allocation \tilde{a} .

Procedure 2. (WHT-BASED ALLOCATION RULE)
i. Use RWHT to compute k -sparse approximations $\tilde{v}_i, i \in N$.
ii. Solve $\tilde{a} \in \arg\max_{a \in \mathcal{F}} \sum_{i \in N} \tilde{v}_i(a_i)$ using Theorem 1.

In Figure 2, we present the efficiency of \tilde{a} on 50 GSVM instances for various values of k . We observe that RWHT achieves a median efficiency of 100% when using 90 or more FCs. Nevertheless, the main practical issue with this approach is the number of value queries required (printed on the top of Figure 2). As we can see, RWHT needs 102,000 value queries (around 39% of all bundles) to find the 90 best FCs. For a practical ICA mechanism this is far too many.

6 A Practical Hybrid ICA Mechanism

In this section, we introduce and experimentally evaluate a practical hybrid ICA mechanism, based on FTs and NNs.

¹For the non-orthogonal FT3 and FT4 we use a heuristic.

²Since the NNs only receive random samples its results should only be understood as a reference point.

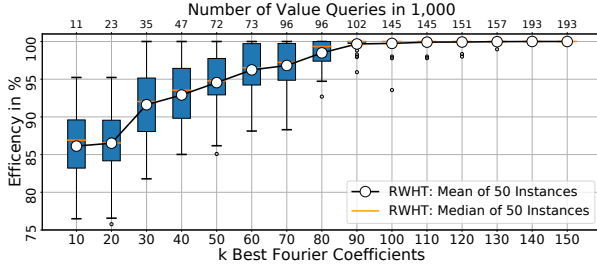


Figure 2: Efficiency of Procedure 2 in GSVM.

6.1 The Hybrid ICA Mechanism

The main issue of the FT-based allocation rule in Section 5.3 is the large number of queries, which we now address. The key idea is the following: instead of directly applying a sparse FT algorithm (like RWHT) to reported value functions, we apply it to a NN-based representation. In this way, we query NNs instead of bidders. Based on the FCs of the NNs, we determine a Fourier-sparse approximation \tilde{v}_i using only *few value queries*, where the idea is that the FCs of each NN concentrate on the most dominant FCs of its corresponding value function. Indeed, recent evidence suggests that a NN trained by SGD can learn the Fourier-support (Rahaman et al. 2019). We analyze our NN-based support discovery rule in Section 6.2. We now present HYBRID ICA, leaving the details of the sub-procedures to Appendix E.1.

HYBRID ICA (Algorithm 3) consists of 3 phases: the *MLCA phase*, the *Fourier reconstruction phase*, and the *Fourier allocation phase*. It is parameterized by an FT F and the numbers $\ell_1, \ell_2, \ell_3, \ell_4$ of different query types. In total, HYBRID ICA asks each bidder $\ell_1 + \ell_2 + \ell_3 + \ell_4$ queries: ℓ_1 random initial, ℓ_2 MLCA allocation, ℓ_3 Fourier reconstruction, and ℓ_4 Fourier allocation queries.

1. MLCA Phase. We first run MLCA such that the NNs can then be trained on “meaningfully” elicited reports. In MLCA, we request reports for ℓ_1 random initial bundles and for ℓ_2 MLCA allocation queries (Lines 1-2).

2. Fourier Reconstruction Phase. Next, we compute a Fourier-sparse approximation \tilde{v}_i . For this, we first fit NN \mathcal{N}_i on the reports R_i (Line 4). Then we compute the best FCs of the fitted NNs (Line 5, **Procedure 3**) in order to discover which FCs might be important to represent the bidders. Then, based on these FCs, we determine ℓ_3 Fourier reconstruction queries \tilde{S}_i (Line 6, **Procedure 4**), which we then send to the bidders and fit \tilde{v}_i to the reports R_i received so far (Line 7, **Procedure 5**).

3. Fourier Allocation Phase. We use the fitted \tilde{v}_i to generate ℓ_4 Fourier allocation queries. Here, we solve the FT-based WDP (Line 9) to get candidate queries q , ensure that all queries are new (Lines 10-14), add the received reports to R_i (Line 15) and refit \tilde{v}_i (Line 16, **Procedure 5**). Finally, based on all reports R , HYBRID ICA computes a welfare-maximizing allocation a_R^* and VCG payments p (Line 17).

Experiment Setup. For HYBRID ICA and MLCA, we use the NN architectures from Weissteiner and Seuken (2020) and set a total query budget of 100 (GSVM and LSVM) and 500 (MRVM). For HYBRID ICA, we optimized the FTs and tried several query parameters $\ell_1, \ell_2, \ell_3, \ell_4$ on a training set

Algorithm 3: HYBRID ICA

Params: F Fourier transform; $\ell_1, \ell_2, \ell_3, \ell_4$ query split

- 1 Set $Q^{\text{init}} = \ell_1$ and $Q^{\text{max}} = \ell_1 + \ell_2$ ▷ MLCA phase
- 2 Run MLCA($Q^{\text{init}}, Q^{\text{max}}$); get $\ell_1 + \ell_2$ reports R
- 3 **foreach** bidder $i \in N$ **do** ▷ Fourier reconstr. phase
- 4 Fit NN \mathcal{N}_i to R_i
- 5 Determine the best FCs of \mathcal{N}_i ▷ Proc. 3
- 6 Compute ℓ_3 reconstruction queries $\tilde{S}_i \subseteq \mathcal{X}$ ▷ Proc. 4
- 7 Ask \tilde{S}_i , add reports to R_i , and fit \tilde{v}_i to R_i ▷ Proc. 5
- 8 **for** $l = 1, \dots, \ell_4$ **do** ▷ Fourier alloc. phase
- 9 Solve $q \in \arg\max_{a \in \mathcal{F}} \sum_{i \in N} \tilde{v}_i(a_i)$ (FT-WDP)
- 10 **foreach** bidder $i \in N$ **do**
- 11 **if** $q_i \in R_i$ **then** ▷ Bundle already queried
- 12 Define $\mathcal{F}' = \{a \in \mathcal{F} : a_i \neq q_i, \forall i \in R_i\}$
- 13 Resolve $q' \in \arg\max_{a \in \mathcal{F}'} \sum_{i \in N} \tilde{v}_i(a_i)$
- 14 Update $q_i = q'_i$
- 15 Query bidder i 's value for q_i and add report to R_i
- 16 Fit \tilde{v}_i to R_i ▷ Proc. 5
- 17 From reports R compute a_R^* as in (1) and VCG payments p
- 18 **return** final allocation a_R^* and VCG payments p

| | NNS ARCHITECTURE | FT | ℓ_1 | ℓ_2 | ℓ_3 | ℓ_4 |
|------|-----------------------------|-----|----------|----------|----------|----------|
| GSVM | R:[32, 32] N:[10, 10] | WHT | 30 | 21 | 20 | 29 |
| LSVM | R:[32, 32] N:[10, 10, 10] | WHT | 30 | 30 | 10 | 30 |
| MRVM | L,R,N:[16, 16] | WHT | 30 | 220 | 0 | 250 |

Table 2: Best configuration of HYBRID ICA. R:[d_1, d_2] denotes a fully-connected 3-hidden-layer NN with ReLU activations for the regional bidder with d_1 , and d_2 nodes.

of CA instances. Table 2 presents the best found configurations. We see that WHT works best for all domains.³

6.2 NNs Support Discovery Experiments

Recall, that in HYBRID ICA we use the NNs as a support discovery method and a key requirement is that the FCs of the NN-based bidders' representation concentrate on the most dominant FCs of its corresponding value function, i.e. the support of the NNs $\text{supp}(\phi_{\mathcal{N}_i})$ fulfills $\text{supp}(\phi_{\mathcal{N}_i}) \approx \text{supp}(\phi_{\tilde{v}_i})$. In the following, we consider the best found configurations from Table 2.

In order to assess the quality of the NN-based support discovery method (Line 5, **Procedure 3**), we consider the spectral *energy ratio* obtained by dividing the spectral energy of the k frequencies selected by the NN-based rule by the spectral energy of the k best frequencies (recall that for the WHT the best FCs are the ones with the largest absolute value). Formally, for each bidder i , we denote the k frequencies selected by our NN-based rule as $\tilde{S}_i = \{\tilde{y}^{(1)}, \dots, \tilde{y}^{(k)}\}$ and the best possible ones by $S_i^* = \{y^{*(1)}, \dots, y^{*(k)}\}$. With this notation in place, bidder i 's *energy ratio* is given by $\sum_{\tilde{y} \in \tilde{S}_i} \phi_{\tilde{v}_i}(\tilde{y})^2 / \sum_{y \in S_i^*} \phi_{\tilde{v}_i}(y)^2 \in [0, 1]$. This ratio is equal to one if $\tilde{S}_i = S_i^*$. Figure 3 shows that, for the considered auction domains, the NN-based rule discovers supports that are almost on par with the best possible supports given a

³Future progress on robust sparse FT3/FT4 algorithms is likely to improve the performance of those FTs in our framework, too.

| MECHANISM | GSVM | | | | | LSVM | | | | | MRVM | | | | | |
|-----------------------|--------------------|------------------|------------------|-------------|---------------|--------------------|------------------|------------------|-------------|---------------|--------------------|---------------|------------------|------------------|-------------|---------------|
| | EFFICIENCY IN % | REGIONAL IN % | NATIONAL IN % | REV IN % | HRS/ INST. | EFFICIENCY IN % | REGIONAL IN % | NATIONAL IN % | REV IN % | HRS/ INST. | EFFICIENCY IN % | LOCAL IN % | REGIONAL IN % | NATIONAL IN % | REV IN % | HRS/ INST. |
| HYBRID ICA | 99.97 ± 0.03 | 94.72 | 5.25 | 81 | 0.81 | 98.74 ± 0.43 | 89.09 | 9.65 | 78 | 1.95 | 96.63 ± 0.31 | 0.00 | 1.19 | 95.44 | 36 | 23.88 |
| MLCA | 99.17 ± 0.37 | 98.11 | 1.06 | 79 | 4.65 | 99.14 ± 0.42 | 93.40 | 5.75 | 77 | 6.09 | 95.32 ± 0.32 | 0.00 | 0.53 | 94.79 | 41 | 43.26 |
| HYBRID ICA (NO FR) | 98.30 ± 0.49 | 97.94 | 0.36 | 75 | 0.93 | 98.16 ± 0.60 | 93.83 | 4.33 | 72 | 2.03 | 96.63 ± 0.31 | 0.00 | 1.19 | 95.44 | 36 | 23.88 |
| HYBRID ICA (NO FR/FA) | 98.16 ± 0.50 | 97.47 | 0.69 | 75 | 0.71 | 97.75 ± 0.63 | 92.78 | 5.27 | 72 | 1.86 | 93.91 ± 0.36 | 0.01 | 0.42 | 93.48 | 42 | 14.68 |
| Efficient Allocation | | 94.75 | 5.25 | | | | 84.03 | 15.97 | | | | 0.00 | 2.11 | 97.89 | | |

Table 3: HYBRID ICA vs. MLCA, HYBRID ICA (NO FR), and HYBRID ICA (NO FR/FA). All results are averages over a test set of 100 (GSVM and LSVM) and 30 (MRVM) CA instances. For efficiency we give a 95% confidence interval and mark the best mechanisms in grey.

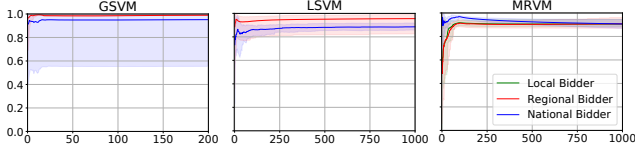


Figure 3: Average energy ratio (y-axis) with 97.5% and 2.5% empirical quantiles for a varying number of selected frequencies k (x-axis) over 30 instances in GSVM and LSVM and over 5 instances in MRVM.

fixed budget of k frequencies. For these plots we removed the WHT-FC corresponding to the zero-frequency, which is equivalent to subtracting the mean from the respective value function. Note that for MRVM we cannot compute the true WHT-FCs, thus we again use RWHT, which recovers the largest WHT-FCs with high probability, instead (details in Appendix E.2).

6.3 Efficiency Experiments

We now evaluate the efficiency of HYBRID ICA and compare it against MLCA in GSVM, LSVM, and MRVM.

Results. Table 3 contains our main results for all three domains. We show efficiency, distribution of efficiency to bidder types, revenue ($\sum_{i \in N} p_i$)/ $V(a^*)$, and run-time. We see that HYBRID ICA outperforms MLCA w.r.t. efficiency in GSVM and MRVM and matches the efficiency of MLCA in LSVM. Furthermore, HYBRID ICA leads to a significant computational speedup ($\times 6$ in GSVM, $\times 3$ in LSVM and $\times 2$ MRVM). Finally, it also distributes the welfare more evenly across bidder types. This also leads to a distribution that more closely resembles that of the efficient allocation (see *Efficient Allocation*). Figure 4 shows the efficiency of the different phases of HYBRID ICA for GSVM (for LSVM and MRVM see Appendix E.3). Starting with 30 random queries, it achieves an (average) efficiency of 66%. Next, our algorithm performs three MLCA iterations to ask 21 *MLCA allocation queries*, resulting in 99 instances having an efficiency of at least 90%. Finally, the Fourier-based queries significantly increase the efficiency from 98.1% to 99.97%.

Fourier queries. To verify the importance of the ℓ_3 Fourier reconstruction and ℓ_4 Fourier allocation queries, we present two comparison mechanisms: HYBRID ICA (NO FR) and HYBRID ICA (NO FR/FA), which use random queries in place of the ℓ_3 Fourier reconstruction and the $\ell_3 + \ell_4$ Fourier-based queries, respectively. As we see in Table 3, using the Fourier queries leads to significantly better efficiency and HYBRID ICA (NO FR/FA) does not achieve a fairer efficiency distribution. Moreover, comparing HYBRID

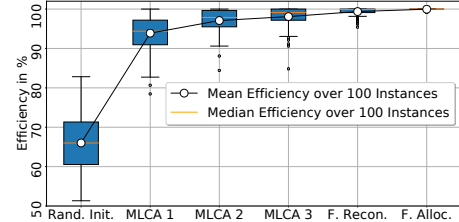


Figure 4: HYBRID ICA in GSVM.

ICA to HYBRID ICA (NO FR) shows that, in GSVM and LSVM, the Fourier reconstruction queries are the main reason for the fairer distribution. We empirically verified that the Fourier reconstruction queries are composed of larger bundles (≈ 17 items compared to ≈ 4 in MLCA queries) and thus allocate large bundles to bidders that would have been overlooked otherwise. In MRVM, the best query split we found for HYBRID ICA uses $\ell_3 = 0$ Fourier reconstruction queries and thus, HYBRID ICA is equal to HYBRID ICA (NO FR). Consequently, in MRVM, HYBRID ICA’s increased efficiency and fairer distribution results from the Fourier allocation queries.

Overall, we see that our Fourier-based approach is especially powerful in sparse domains. In practice, bidders are often limited by their cognitive abilities (Scheffel, Ziegler, and Bichler 2012) or use a (low-dimensional) computational model to represent their value function. Thus, their revealed preferences typically exhibit only a limited degree of substitutability and complementarity, which is captured well by Fourier-sparsity.

7 Conclusion

In this paper, we have introduced Fourier analysis for the design of CAs. The main idea was to represent value functions using Fourier-sparse approximations, providing us with a new lens on bidder’s values in the Fourier domain.

On a technical level, our main contribution was to derive succinct MIPs for the Fourier transform-based WDPs, which makes computing Fourier-based allocation queries practically feasible. We have leveraged this to design a new hybrid ICA mechanism that uses NN-based and Fourier-based queries. Our experiments have shown that our approach leads to higher efficiency than the current benchmark, while achieving a significant computational speedup and a fairer distribution of social welfare among bidders.

With this paper, we have laid the foundations for future work leveraging Fourier analysis for representing and eliciting preferences in combinatorial settings. We envision exciting applications in course allocation and social choice.

8 Acknowledgments

This paper is part of a project that has received funding from the European Research Council (ERC) under the European Union’s Horizon 2020 research and innovation programme (Grant agreement No. 805542). This material is based upon work supported by the National Science Foundation under grant no. CMMI-1761163.

References

- Abraham, I.; Babaioff, M.; Dughmi, S.; and Roughgarden, T. 2012. Combinatorial auctions with restricted complements. In *Proceedings of the 13th ACM Conference on Electronic Commerce*, 3–16.
- Amrollahi, A.; Zandieh, A.; Kapralov, M.; and Krause, A. 2019. Efficiently learning Fourier sparse set functions. In *Advances in Neural Information Processing Systems*, 15120–15129.
- Ausubel, L.; and Cramton, P. 2011. Auction design for wind rights. *Report to Bureau of Ocean Energy Management, Regulation and Enforcement*.
- Ausubel, L. M.; and Baranov, O. 2017. A practical guide to the combinatorial clock auction. *Economic Journal*, 127(605): F334–F350.
- Ausubel, L. M.; Cramton, P.; and Milgrom, P. 2006. The clock-proxy auction: A practical combinatorial auction design. In Cramton, P.; Shoham, Y.; and Steinberg, R., eds., *Combinatorial Auctions*, 115–138. MIT Press.
- Bernasconi, A.; Codenotti, B.; and Simon, J. 1996. On the Fourier analysis of Boolean functions. *preprint*, 1–24.
- Blum, A.; Jackson, J.; Sandholm, T.; and Zinkevich, M. 2004. Preference elicitation and query learning. *Journal of Machine Learning Research*, 5: 649–667.
- Brero, G.; Lahaie, S.; and Seuken, S. 2019. Fast Iterative Combinatorial Auctions via Bayesian Learning. In *Proceedings of the 33rd AAAI Conference of Artificial Intelligence*.
- Brero, G.; Lubin, B.; and Seuken, S. 2018. Combinatorial Auctions via Machine Learning-based Preference Elicitation. In *Proceedings of the 27th International Joint Conference on Artificial Intelligence*.
- Brero, G.; Lubin, B.; and Seuken, S. 2021. Machine Learning-powered Iterative Combinatorial Auctions. *arXiv preprint arXiv:1911.08042*.
- Dütting, P.; Feng, Z.; Narasimhan, H.; Parkes, D. C.; and Ravindranath, S. S. 2019. Optimal auctions through deep learning. In *Proceedings of the 36th International Conference on Machine Learning*.
- Efron, B.; Hastie, T.; Johnstone, I.; Tibshirani, R.; et al. 2004. Least angle regression. *The Annals of statistics*, 32(2): 407–499.
- Goeree, J. K.; and Holt, C. A. 2010. Hierarchical package bidding: A paper & pencil combinatorial auction. *Games and Economic Behavior*, 70(1): 146–169.
- Lahaie, S. 2010a. Kernel Methods for Revealed Preference Analysis. In *ECAI*, 439–444.
- Lahaie, S. 2010b. Stability and incentive compatibility in a kernel-based combinatorial auction. In *Proceedings of the AAAI Conference on Artificial Intelligence*, volume 24.
- Lahaie, S. M.; and Parkes, D. C. 2004. Applying learning algorithms to preference elicitation. In *Proceedings of the 5th ACM Conference on Electronic Commerce*.
- Nisan, N.; and Segal, I. 2006. The communication requirements of efficient allocations and supporting prices. *Journal of Economic Theory*, 129(1): 192–224.
- O’Donnell, R. 2014. *Analysis of boolean functions*. Cambridge University Press.
- Püschel, M.; and Wendler, C. 2020. Discrete Signal Processing with Set Functions. *arXiv preprint arXiv:2001.10290*.
- Rahaman, N.; Baratin, A.; Arpit, D.; Draxler, F.; Lin, M.; Hamprecht, F.; Bengio, Y.; and Courville, A. 2019. On the spectral bias of neural networks. In *International Conference on Machine Learning*, 5301–5310. PMLR.
- Rahme, J.; Jelassi, S.; Bruna, J.; and Weinberg, S. M. 2020. A Permutation-Equivariant Neural Network Architecture For Auction Design. *arXiv preprint arXiv:2003.01497*.
- Scheffel, T.; Ziegler, G.; and Bichler, M. 2012. On the impact of package selection in combinatorial auctions: an experimental study in the context of spectrum auction design. *Experimental Economics*, 15(4): 667–692.
- Stobbe, P.; and Krause, A. 2012. Learning Fourier sparse set functions. In *Artificial Intelligence and Statistics*, 1125–1133.
- Weiss, M.; Lubin, B.; and Seuken, S. 2017. Sats: A universal spectrum auction test suite. In *Proceedings of the 16th Conference on Autonomous Agents and Multi-Agent Systems*.
- Weissteiner, J.; and Seuken, S. 2020. Deep Learning-powered Iterative Combinatorial Auctions. In *Proceedings of the 34th AAAI Conference of Artificial Intelligence*.
- Wendler, C.; Amrollahi, A.; Seifert, B.; Krause, A.; and Püschel, M. 2020. Learning Set Functions that are Sparse in Non-Orthogonal Fourier Bases. *arXiv preprint arXiv:2010.00439*.

Appendix

A Preliminaries

In this section, we provide a recap on how to compute VCG payments from bidder’s reports.

A.1 VCG Payments from Reports

Let $R = (R_1, \dots, R_n)$ denote an elicited set of reported bundle-value pairs from each bidder obtained from MLCA (Algorithm 2) or HYBRID ICA (Algorithm 3) and let $R_{-i} := (R_1, \dots, R_{i-1}, R_{i+1}, \dots, R_n)$. We then calculate the VCG payments $p = (p_1, \dots, p_n) \in \mathbb{R}_+^n$ as follows:

Definition 2. (VCG PAYMENTS FROM REPORTS)

$$p_i := \sum_{j \in N \setminus \{i\}} \hat{v}_j \left(\left(a_{R_{-i}}^* \right)_j \right) - \sum_{j \in N \setminus \{i\}} \hat{v}_j \left(\left(a_R^* \right)_j \right). \quad (22)$$

where a_{R-i}^* maximizes the reported social welfare when excluding bidder i , i.e.,

$$a_{R-i}^* \in \operatorname{argmax}_{a \in \mathcal{F}} \widehat{V}(a|R_{-i}) = \operatorname{argmax}_{a \in \mathcal{F}} \sum_{\substack{j \in N \setminus \{i\}: \\ (a_j, \hat{v}_j(a_j)) \in R_j}} \hat{v}_j(a_j), \quad (23)$$

and a_R^* is a reported-social-welfare-maximizing allocation (including all bidders), i.e.,

$$a_R^* \in \operatorname{argmax}_{a \in \mathcal{F}} \widehat{V}(a|R) = \operatorname{argmax}_{a \in \mathcal{F}} \sum_{i \in N: (a_i, \hat{v}_i(a_i)) \in R_i} \hat{v}_i(a_i). \quad (24)$$

As argued in Brero, Lubin, and Seuken (2021), using such payments are key for MLCA to induce “good” incentives for bidders to report truthfully. As their incentive analysis also applies to HYBRID ICA, we use them in our design too.

B Fourier Analysis of Value Functions

The benefit of considering multiple FTs is that they offer different, non-equivalent notions of sparsity as illustrated by the following example.

Example 1. Consider the set of items $M = \{1, 2, 3\}$ and the associated reported value function \hat{v}_i shown in Table 4 (where we use 001 as a shorthand notation for $(0, 0, 1)$), together with the corresponding FCs $\phi_{\hat{v}_i}$. This bidder exhibits

| | 000 | 100 | 010 | 001 | 110 | 101 | 011 | 111 |
|-------------|------|------|------|------|-----|-----|-----|-----|
| \hat{v}_i | 0 | 1 | 1 | 1 | 3 | 3 | 3 | 5 |
| FT3 | 0 | 1 | 1 | 1 | 1 | 1 | 1 | -1 |
| FT4 | 5 | -2 | -2 | -2 | 0 | 0 | 0 | 1 |
| WHT | 17/8 | -7/8 | -7/8 | -7/8 | 1/8 | 1/8 | 1/8 | 1/8 |

Table 4: Example with different induced notions of sparsity of all considered FTs.

complementary effects for each bundle containing more than one item, as can be seen, e.g., from $3 = \hat{v}_i(110) > \hat{v}_i(100) + \hat{v}_i(010) = 2$ and $5 = \hat{v}_i(111) > \hat{v}_i(100) + \hat{v}_i(010) + \hat{v}_i(001) = 3$. Observe that while this value function is sparse in FT4, i.e., $\phi_{\hat{v}_i}(110) = \phi_{\hat{v}_i}(101) = \phi_{\hat{v}_i}(011) = 0$, it is neither sparse in FT3 nor WHT. Note that the coefficients $\phi_{\hat{v}_i}(100)$, $\phi_{\hat{v}_i}(010)$, and $\phi_{\hat{v}_i}(001)$ capture the value of single items and thus cannot be zero.

The induced spectral energy distributions for each FT, i.e., for each cardinality (i.e., number of items) d from 0 to $m = 3$, we compute $\sum_{y \in \mathcal{X}: |y|=d} \phi_{\hat{v}_i}(y)^2 / \sum_{y \in \mathcal{X}} \phi_{\hat{v}_i}(y)^2$, are shown in Table 5.

| | $d = 0$ | $d = 1$ | $d = 2$ | $d = 3$ |
|-----|---------|---------|---------|---------|
| FT3 | 0.00 | 42.86 | 42.86 | 14.28 |
| FT4 | 65.79 | 31.58 | 0.00 | 2.63 |
| WHT | 65.69 | 33.41 | 0.68 | 0.22 |

Table 5: Spectral energy in % for each cardinality (i.e., number of items) d from 0 to $m = 3$ of all considered FTs.

C Fourier Transform-based WDPs

In this Section, we present the proofs of Lemma 1 and Theorem 1.

Let 1_d and 0_d for $d \in \mathbb{N}$ denote the d -dimensional vector of ones and zeros, respectively. For all $x, y \in \mathbb{R}^d$, let $x \leq y$, $\max(x, y)$, $\min(x, y)$ and $(-1)^x$ be defined component-wise, and let $\langle \cdot, \cdot \rangle$ denote the Euclidean scalar product.

We consider the matrix representation F and F^{-1} of the considered FTs from Püschel and Wendler (2020) given by:

$$\text{FT3: } F_{y,x} = (-1)^{|y|-|x|} \mathbb{I}_{\min(x,y)=x}, \quad (25)$$

$$F_{x,y}^{-1} = \mathbb{I}_{\min(x,y)=y}, \quad (26)$$

$$\text{FT4: } F_{y,x} = (-1)^{|\min(x,y)|} \mathbb{I}_{\max(x,y)=1_m}, \quad (27)$$

$$F_{x,y}^{-1} = \mathbb{I}_{\min(x,y)=0_m}, \quad (28)$$

$$\text{WHT: } F_{y,x} = \frac{1}{2^m} (-1)^{|\min(x,y)|}, \quad (29)$$

$$F_{x,y}^{-1} = (-1)^{|\min(x,y)|}. \quad (30)$$

The Fourier-sparse approximations used in the WDPs are defined in terms of F^{-1} .

C.1 Proof of Lemma 1

Lemma 1. (SUCCINCT REPRESENTATIONS) For $i \in N$ let $\mathcal{S}_i = \{y^{(1)}, \dots, y^{(k)}\}$ be the support of a k -Fourier-sparse approximation \tilde{v}_i and $W_i \in \{0, 1\}^{k \times m}$ be defined as $(W_i)_{l,j} = \mathbb{I}_{y_j^{(l)}=1}$. Then \tilde{v}_i can be rewritten as:

$$\text{FT3: } \tilde{v}_i(x) = \langle \phi_{\tilde{v}_i|\mathcal{S}_i}, \max(0_k, 1_k - W_i(1_m - x)) \rangle \quad (31)$$

$$\text{FT4: } \tilde{v}_i(x) = \langle \phi_{\tilde{v}_i|\mathcal{S}_i}, \max(0_k, 1_k - W_i x) \rangle \quad (32)$$

$$\text{WHT: } \tilde{v}_i(x) = \langle \phi_{\tilde{v}_i|\mathcal{S}_i}, (-1)^{W_i x} \rangle. \quad (33)$$

Proof. In this proof we are going to make use of the equivalence between bundles (= indicator vectors) and sets. Recall that $x, y \in \mathcal{X} = \{0, 1\}^m$ are bundles and bundles correspond to subsets of items. We can translate set operations such as intersection, union and complement to indicator vectors as follows:

$$x \cap y = \min(x, y), \quad (34)$$

$$x \cup y = \max(x, y), \quad (35)$$

$$(x)^c = 1_m - x, \quad (36)$$

where we slightly abused notation by identifying the indicator vectors with their corresponding subsets on the left hand sides of (34)–(36). Furthermore, it holds that:

$$|\min(x, y)| = y^T x = \sum_{i=1}^m x_i y_i \quad (37)$$

FT3. Let F denote the matrix representation of FT3 in

(25). By definition, we have

$$\tilde{v}_i(x) = \sum_{y \in \mathcal{S}_i} F_{x,y}^{-1} \phi_{\tilde{v}_i}(y) \quad (38)$$

$$= \sum_{y \in \mathcal{S}_i} \mathbb{I}_{\min(x,y)=y} \phi_{\tilde{v}_i}(y) \quad (39)$$

$$= \sum_{y \in \mathcal{S}_i} \mathbb{I}_{\min(1_m-x,y)=0_m} \phi_{\tilde{v}_i}(y) \quad (40)$$

$$= \langle (\mathbb{I}_{\min(1_m-x,y)=0_m})_{y \in \mathcal{S}_i}, \phi_{\tilde{v}_i}|_{\mathcal{S}_i} \rangle, \quad (41)$$

where we used $x \cap y = y \Leftrightarrow x^c \cap y = \emptyset$. Now, the claim follows by observing that

$$\mathbb{I}_{\min(1_m-x,y)=0_m} = \max(0, 1 - y^T(1_m - x)), \quad (42)$$

which is a direct consequence of $|\min(1_m - x, y)| = y^T(1_m - x)$, and recalling that for each $y \in \mathcal{S}_i$ there is a respective row y^T in W_i .

FT4. Let F be the matrix representation of FT4 in (27). By definition, we have

$$\tilde{v}_i(x) = \sum_{y \in \mathcal{S}_i} F_{x,y}^{-1} \phi_{\tilde{v}_i}(y) \quad (43)$$

$$= \sum_{y \in \mathcal{S}_i} \mathbb{I}_{\min(x,y)=0_m} \phi_{\tilde{v}_i}(y) \quad (44)$$

$$= \langle (\mathbb{I}_{\min(x,y)=0_m})_{y \in \mathcal{S}_i}, \phi_{\tilde{v}_i}|_{\mathcal{S}_i} \rangle. \quad (45)$$

Now, the claim follows by observing that

$$\mathbb{I}_{\min(x,y)=0_m} = \max(0, 1 - y^T x), \quad (46)$$

which is a direct consequence of $|\min(x, y)| = y^T x$, and recalling that for each $y \in \mathcal{S}_i$ there is a respective row y^T in W_i .

WHT. Let F be the matrix representation of WHT in (29). By definition, we have

$$\tilde{v}_i(x) = \sum_{y \in \mathcal{S}_i} F_{x,y}^{-1} \phi_{\tilde{v}_i}(y) \quad (47)$$

$$= \sum_{y \in \mathcal{S}_i} (-1)^{y^T x} \phi_{\tilde{v}_i}(y) \quad (48)$$

$$= \langle ((-1)^{y^T x})_{y \in \mathcal{S}_i}, \phi_{\tilde{v}_i}|_{\mathcal{S}_i} \rangle. \quad (49)$$

Now, the claim follows by recalling that for each $y \in \mathcal{S}_i$ there is a respective row y^T in W_i . \square

C.2 Proof of Theorem 1

We first state and proof two elementary lemmata.

For $x \in \mathbb{R}^d$ let $x \pmod{2}$ be defined component-wise.

Lemma 2. (MAX REPRESENTATION) *Let $\zeta, \eta \in \mathbb{R}^d$ for $d \in \mathbb{N}$ and $C > 0$ such that for all $l \in \{1, \dots, d\}$ it holds that $|\zeta_l - \eta_l| \leq C$. Let $\alpha := \max(\zeta, \eta)$ and consider the polytope \mathcal{P} in $(\tilde{\alpha}, \beta)$ defined by (50)–(54)*

$$\tilde{\alpha} \geq \eta \quad (50)$$

$$\tilde{\alpha} \leq \eta + C\beta \quad (51)$$

$$\tilde{\alpha} \geq \zeta \quad (52)$$

$$\tilde{\alpha} \leq \zeta + C(1_d - \beta) \quad (53)$$

$$\beta \in \{0, 1\}^d. \quad (54)$$

Then it holds that $\mathcal{P} \neq \emptyset$ and every element $(\tilde{\alpha}, \beta) \in \mathcal{P}$ satisfies $\tilde{\alpha} = \alpha$.

Proof. Non-emptiness follows from the assumption that $|\zeta_l - \eta_l| \leq C$ for all $l \in \{1, \dots, d\}$. For any $l \in \{1, \dots, d\}$ we have to distinguish the following cases:

$$\zeta_l < \eta_l \implies \beta_l = 0, \tilde{\alpha}_l = \eta_l = \max(\zeta_l, \eta_l) = \alpha_l$$

$$\zeta_l > \eta_l \implies \beta_l = 1, \tilde{\alpha}_l = \zeta_l = \max(\zeta_l, \eta_l) = \alpha_l$$

$$\zeta_l = \eta_l \implies \tilde{\alpha}_l = \zeta_l = \eta_l = \max(\zeta_l, \eta_l) = \alpha_l$$

This yields that $\tilde{\alpha} = \alpha$. \square

Lemma 3. (ODD-EVEN REPRESENTATION) *Let $\zeta \in \mathbb{Z}^d$ for $d \in \mathbb{N}$. Let $\beta := \zeta \pmod{2} \in \{0, 1\}^d$ and consider the polytope \mathcal{P} in $(\tilde{\beta}, \gamma)$ defined by (55) and (56)*

$$\tilde{\beta} = \zeta - 2\gamma \quad (55)$$

$$\tilde{\beta} \in \{0, 1\}^d, \gamma \in \mathbb{Z}^d. \quad (56)$$

Then it holds that $\mathcal{P} \neq \emptyset$ and every element $(\tilde{\beta}, \gamma) \in \mathcal{P}$ satisfies $\tilde{\beta} = \beta$.

Proof. Non-emptiness follows since $\zeta \in \mathbb{Z}^d$ per assumption. For any $l \in \{1, \dots, d\}$ we have to distinguish the following cases:

$$\zeta_l \pmod{2} = 0 \implies \gamma_l = \frac{\zeta_l}{2}, \tilde{\beta}_l = 0 = \beta_l$$

$$\zeta_l \pmod{2} = 1 \implies \gamma_l = \frac{\zeta_l - 1}{2}, \tilde{\beta}_l = 1 = \beta_l$$

Thus $\tilde{\beta} = \beta$. \square

For each bidder $i \in N$ let $\tilde{v}_i : \mathcal{X} \rightarrow \mathbb{R}_+$ be the Fourier-sparse approximation of the bidder's reported value function \hat{v}_i . Then the *Fourier transform-based WDP* was defined as follows:

Definition 3. (FOURIER TRANSFORM-BASED WDP)

$$\operatorname{argmax}_{a \in \mathcal{F}} \sum_{i \in N} \tilde{v}_i(a_i). \quad (\text{FT-WDP})$$

Next, we proof Theorem 1.

Theorem 1. (FOURIER TRANSFORM-BASED MIPs) *Let $\tilde{v}_i : \mathcal{X} \rightarrow \mathbb{R}$ be a k -Fourier-sparse approximation as defined in (31), (32), or (33). Then there exists a constant $C > 0$ such that the MIP defined by the following objective*

$$\operatorname{argmax}_{a \in \mathcal{F}, \beta_i \in \{0, 1\}^k} \sum_{i \in N} \langle \phi_{\tilde{v}_i}|_{\mathcal{S}_i}, \alpha_i \rangle, \quad (57)$$

and for $i \in N$ one set of transform specific constraints (58)–(60), or (61)–(63), or (64)–(66), is equivalent to (FT-WDP).

$$\text{FT3:} \quad \text{s.t. } \alpha_i \geq 1_k - W_i(1_m - a_i) \quad (58)$$

$$\alpha_i \leq 1_k - W_i(1_m - a_i) + C\beta_i \quad (59)$$

$$0_k \leq \alpha_i \leq C(1_k - \beta_i) \quad (60)$$

$$\text{FT4:} \quad \text{s.t. } \alpha_i \geq 1_k - W_i a_i \quad (61)$$

$$\alpha_i \leq 1_k - W_i a_i + C\beta_i \quad (62)$$

$$0_k \leq \alpha_i \leq C(1_k - \beta_i) \quad (63)$$

$$\text{WHT:} \quad \text{s.t. } \alpha_i = -2\beta_i + 1_k \quad (64)$$

$$\beta_i = W_i a_i - 2\gamma_i \quad (65)$$

$$\gamma_i \in \mathbb{Z}^k \quad (66)$$

Proof. We proof the equivalence for each of the FTs and corresponding MIPs separately.

• **FT3**

Let $C > 0$ such that $|[1_k - W_i(1_m - a_i)]_l| \leq C$ for all $l \in \{1, \dots, k\}$, $i \in N$, and $a \in \mathcal{F}$. We then define

$$\alpha_i := \max(0_k, 1_k - W_i(1_m - a_i)) \text{ for all } i \in N,$$

and apply for each α_i Lemma 2 to $\zeta := 0_k$ and $\eta := 1_k - W_i(1_m - a_i)$, which concludes the proof for FT3.

• **FT4:**

This follows analogously as for the FT3 when defining $\alpha_i := \max(0_k, 1_k - W_i a_i)$, $\zeta := 0_k$ and $\eta := 1_k - W_i a_i$.

• **WHT:**

Since for all $i \in N$ and $a \in \mathcal{F}$ it holds that $W_i a_i \in \mathbb{Z}^k$, an immediate consequence from Lemma 3 is that $\beta_i = W_i a_i \pmod{2}$ and $(-1)^{W_i a_i} = -2\beta_i + 1_k$, which concludes the proof for the WHT. \square

D Analyzing the Potential of a FT-based CA

D.1 Fourier Sparsity - GSVM and MRVM

In this Section, we provide the Fourier sparsity results for GSVM and MRVM. In Figure 5, we present the mean over 30 GSVM instances and bidder types. Figure 5 shows that GSVM is low degree ≤ 2 in all considered FTs and thus can be represented using less or equal to $172 = \binom{18}{0} + \binom{18}{1} + \binom{18}{2}$ FCs with any FT.

To the best of our knowledge it is not possible to compute the exact FCs with respect to any of the considered FTs for all MRVM bidders (see Wendler et al. (2020)). In Figure 6 we thus depict the *approximate* WHT-energy-distribution for MRVM. In order to do so, we used the RWHT algorithm by (Amrollahi et al. 2019), which recovers the largest WHT-FCs with high probability. Note that here we don't normalize by the total energy since the total energy is an unknown quantity in the space of 2^{98} bundles.

Figure 6 shows the *approximate* WHT-energy-distribution for MRVM. We see that while most of the energy is contained in the low degree FCs ≤ 2 , there is still some non negligible energy in the FCs of degree 3–7.

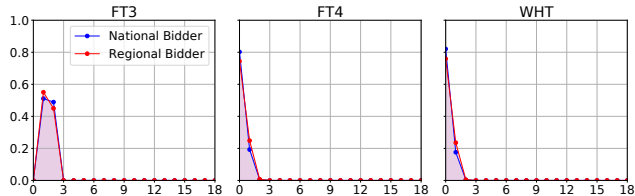


Figure 5: Spectral energy distribution in GSVM for different notions of FTs. For each cardinality (x-axis), we collect the spectral energy (y-axis) of all frequencies of that cardinality and normalize by the total spectral energy.

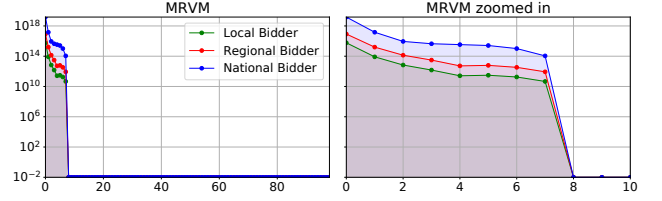


Figure 6: Approximate spectral energy distribution in MRVM for WHT computed with the robust WHT algorithm from (Amrollahi et al. 2019). For each cardinality (x-axis), we collect the spectral energy (y-axis) of all frequencies of that cardinality.

D.2 Reconstruction Error of Fourier Transforms

Using Procedure 1, we determine the best k -Fourier-sparse approximation \tilde{v}_i for all considered FTs.

Procedure 1. (BEST FCs GIVEN FULL ACCESS TO \hat{v}_i)

Compute all FCs by using the full FT for each bidders' reported value function $\phi_{\hat{v}_i} = F\hat{v}_i$. Next, determine the k best FCs $\phi_{\hat{v}_i|S_i}$ in terms of L2 error $\|\hat{v}_i - \tilde{v}_i\|_2^2$ as follows:

- WHT:** use the FCs with the k largest absolute values.
- FT3 and FT4:** use the FCs with the k largest coefficients $|\phi_{\hat{v}_i}(y)|\|F_{\cdot,y}^{-1}\|_2$, where $F_{\cdot,y}^{-1}$ denotes the y^{th} column.

In the following, we present the technical details for i. and ii..

Let F denote the corresponding matrix representation of the FT3, FT4, or the WHT. Furthermore, fix bidder $i \in N$ and for $S_i \subseteq \text{supp}(\phi_{\hat{v}_i})$, $|S_i| = k \ll 2^m$ let

$$\tilde{v}_i = \sum_{y \in S_i} F_{x,y}^{-1} \phi_{\hat{v}_i}(y) = F_{\cdot,S_i}^{-1} \phi_{\hat{v}_i|S_i},$$

be a k -Fourier-sparse approximation, where we denote by F_{\cdot,S_i}^{-1} the sub matrix of F^{-1} obtained by selecting the columns indexed by the bundles in S_i .

Best Fourier Coefficients WHT For the WHT, we consider the following optimization problem of selecting the k -best FCs with respect to the quadratic error:

$$S_i^* \in \underset{S_i \subseteq \text{supp}(\phi_{\hat{v}_i}), |S_i|=k}{\text{argmin}} \|\hat{v}_i - F_{\cdot,S_i}^{-1} \phi_{\hat{v}_i|S_i}\|_2^2. \quad (67)$$

Then, it follows that S_i^* consists out of those bundles $\{y^{(l)}\}_{l=1}^k$ with the largest absolute value of the corresponding FCs $\{\phi_{\hat{v}_i}(y^{(l)})\}_{l=1}^k$. This can be seen as follows.

$$\|\hat{v}_i - \underbrace{F_{\cdot,S_i}^{-1} \phi_{\hat{v}_i|S_i}}_{\tilde{v}_i}\|_2^2 = \left\| \sum_{y \notin S_i} F_{\cdot,y}^{-1} \phi_{\hat{v}_i}(y) \right\|_2^2 = \quad (68)$$

$$= \sum_{x, y \notin S_i} \langle F_{\cdot,x}^{-1}, F_{\cdot,y}^{-1} \rangle \phi_{\hat{v}_i}(x) \phi_{\hat{v}_i}(y) = \quad (69)$$

$$= \sum_{y \notin S_i} \phi_{\hat{v}_i}(y)^2, \quad (70)$$

where in the last equality we used that F^{-1} is an orthogonal matrix and thus its columns fulfill $\langle F_{\cdot,x}^{-1}, F_{\cdot,y}^{-1} \rangle = \mathbb{I}_{x=y}$.

For the other non-orthogonal transforms FT3 and FT4, we use a heuristic based on the triangular inequality to select the k “best” FCs, which we present next.

Best Fourier Coefficients FT3 and FT4 For FT3 and FT4, we use the triangular inequality

$$\|\hat{v}_i - \underbrace{F_{\cdot, \mathcal{S}_i}^{-1} \phi_{\hat{v}_i|_{\mathcal{S}_i}}}_{\tilde{v}_i}\|_2 \leq \sum_{y \notin \mathcal{S}_i} |\phi_{\hat{v}_i}(y)| \|F_{\cdot, y}^{-1}\|_2$$

to get an upper bound of the quadratic error $\|\hat{v}_i - \tilde{v}_i\|_2^2$ and select the FCs with the k largest coefficients $|\phi_{\hat{v}_i}(y)| \|F_{\cdot, y}^{-1}\|_2$, where $F_{\cdot, y}^{-1}$ denotes the y^{th} column of F^{-1} .

E A Practical Hybrid ICA Mechanism

E.1 Technical Details of HYBRID ICA

In this section we provide the technical details for the implementation of HYBRID ICA. In particular, we explain in more detail the Fourier Transform-based procedures 3–5.

Determining the best FCs of NN

Procedure 3. (BEST FCS OF NEURAL NETWORKS)

- i. If $m \leq 29$: calculate the full FT of the NNs and select the best FCs.
- ii. If $m > 29$: use sparse FT algorithms, i.e., RWHT for WHT and SSFT (Wendler et al. 2020) for FT3 and FT4 to obtain the best FCs of the NNs.

Using **Procedure 3** we determine the best FCs of the NN estimates of each bidder. We distinguish the two cases:

- **Small number of items:** if the number of items is small enough, i.e., $m \leq 29$, we determine the best FCs (and associated locations $\mathcal{S}_i \subset \mathcal{X}$) of \mathcal{N}_i for all FTs by computing its full Fourier transform $F\mathcal{N}_i = \phi_{\mathcal{N}_i}$ using the respective algorithms from Püschel and Wendler (2020).
- **Large number of items:** if the number of items is too large, i.e., $m > 29$, we cannot compute the full Fourier transform and thus require sparse FT algorithms to compute the locations of the best FCs. For the WHT, we can do so by using the *robust sparse WHT algorithm (RWHT)* by Amrollahi et al. (2019). For FT3 and FT4, we use the *sparse set function Fourier transform (SSFT)* algorithm by Wendler et al. (2020). Both algorithms compute Fourier-sparse approximations by only using queries from the corresponding set function (= a bidder's value function), and thus do not require a representation of the exponentially large full set function.
- **Best WHT FCs:** for the WHT the best FCs are the ones with the largest absolute values (see Section D.2). We select the locations of the ℓ_{superset} best NN FCs, i.e., $|\mathcal{S}_i| = \ell_{\text{superset}}$. We do so because we are going to use the *compressive sensing method* by Stobbe and Krause (2012), which only requires a superset of the support $\text{supp}(\phi_{\hat{v}_i})$, in **Procedure 5** to fit the Fourier-sparse approximations \tilde{v}_i to the bidders' reports R_i . In our experiments, we set $\ell_{\text{superset}} = 2,000$ for all domains. Ideally, we would like to choose ℓ_{superset} as large as possible to ensure that the best NN FCs actually overlap with the best FCs of \hat{v}_i , however, there is a trade-off between the number of samples (and also running time) required by the *compressive sensing method* and the size of the support superset. We did not optimize this hyperparameter.

- **Best FT3 and FT4 FCs:** for the FT3 and FT4 we use a heuristic based on the triangular inequality to select the best FCs and their locations (see Section D.2). As neither FT3 nor FT4 are orthogonal or satisfy the restricted isometry property required by the *compressive sensing method*, we only take the best ℓ_3 locations of NN FCs, i.e., $|\mathcal{S}_i| = \ell_3$.

Notice that the goal of **Procedure 3** is solely to determine a set of bundles $\mathcal{S}_i \subseteq \mathcal{X}$ that is likely to contain many of the dominant FCs of \hat{v}_i . This set \mathcal{S}_i is then used to determine reconstructing queries $\tilde{\mathcal{S}}_i$.

Determining reconstruction queries

Procedure 4. (FOURIER RECONSTRUCTION QUERIES)

- i. **FT3 and FT4:** use the sampling theorems by Püschel and Wendler (2020) to determine queries for the bidders, i.e., bundles $\tilde{\mathcal{S}}_i \subseteq \mathcal{X}$, that enable a reconstruction of \tilde{v}_i .
- ii. **WHT:** use the same queries as for FT4.

We make use of the sampling theorems for FT3 and FT4 presented by Püschel and Wendler (2020) to obtain reconstruction queries, i.e., queries that help obtaining a small reconstruction error $\|\hat{v}_i - \tilde{v}_i\|_2$. Our rationale here is that the queries given by the sampling theorem $\tilde{\mathcal{S}}_i$ would lead to $\|\hat{v}_i - \tilde{v}_i\|_2 = 0$ for $\text{supp}(\phi_{\hat{v}_i}) = \mathcal{S}_i$. The sampling theorem by Püschel and Wendler (2020) selects rows $\tilde{\mathcal{S}}_i$ such that $F_{\tilde{\mathcal{S}}_i, \mathcal{S}_i}^{-1}$ is of full rank, because then (iff $\text{supp}(\phi_{\hat{v}_i}) = \mathcal{S}_i$) the Fourier coefficients $\phi_{\hat{v}_i|_{\mathcal{S}_i}}$ are the solution of the linear system of equations $\hat{v}_i|_{\mathcal{S}_i} = F_{\tilde{\mathcal{S}}_i, \mathcal{S}_i}^{-1} \phi_{\hat{v}_i|_{\mathcal{S}_i}}$. In particular, the theorem yields

- **FT3:** $\tilde{\mathcal{S}}_i = \mathcal{S}_i$,
- **FT4:** $\tilde{\mathcal{S}}_i = \{1_m - y : y \in \mathcal{S}_i\}$.

For the WHT there is no sampling theorem and we use

$$\tilde{\mathcal{S}}_i = \{1_m - y : |\phi_{\mathcal{N}_i}(y)| \text{ is in the } \ell_3 \text{ largest in } \mathcal{S}_i\}$$

as a heuristic to obtain reconstruction queries. Choosing $\tilde{\mathcal{S}}_i$ in that way empirically often leads to a full-rank submatrix $F_{\tilde{\mathcal{S}}_i, \mathcal{Z}}^{-1}$ of the inverse WHT obtained by selecting the rows indexed by $\tilde{\mathcal{S}}_i$ and the columns indexed by \mathcal{Z} , where $\mathcal{Z} \subseteq \mathcal{S}_i$ are the locations of the ℓ_3 in absolute value largest FCs in \mathcal{S}_i , i.e., $\mathcal{Z} := \{y : |\phi_{\mathcal{N}_i}(y)| \text{ is in the } \ell_3 \text{ largest in } \mathcal{S}_i\}$. If $F_{\tilde{\mathcal{S}}_i, \mathcal{Z}}^{-1}$ is full rank and $\text{supp}(\phi_{\hat{v}_i}) = \mathcal{Z}$, the Fourier coefficients $\phi_{\hat{v}_i|_{\mathcal{Z}}}$ are the solution of the linear system of equations $\hat{v}_i|_{\mathcal{S}_i} = F_{\tilde{\mathcal{S}}_i, \mathcal{Z}}^{-1} \phi_{\hat{v}_i|_{\mathcal{Z}}}$.

Fitting the Fourier-sparse approximations

Procedure 5. (FIT FOURIER-SPARSE \tilde{v}_i TO REPORTS)

- i. **FT3 and FT4:** solve the least squares problem defined by the best FCs and reports R_i .
- ii. **WHT:** use the compressive sensing method by Stobbe and Krause (2012) defined by the best FCs and reports R_i .

Lastly, we need to fit our Fourier-sparse approximations \tilde{v}_i with $\text{supp}(\phi_{\hat{v}_i}) = \mathcal{S}_i$ to the elicited reports $R_i :=$

$\{(x^{(l)}, \hat{v}_i(x^{(l)}))\}$. That is, we determine values $w \in \mathbb{R}^{|\mathcal{S}_i|}$ for the FCs of the Fourier-sparse approximation $\hat{v}_i = F_{\cdot, \mathcal{S}_i}^{-1} w$.

- **WHT:** as already mentioned, for the WHT this is done using the *compressive sensing method* by [Stobbe and Krause \(2012\)](#). We calculate the full regularization path for the L1-regularization parameter λ using the LARS method from [Efron et al. \(2004\)](#), and select the λ that yields ℓ_{support} non zero FCs. In our experiments we set $\ell_{\text{support}} = 100$ in GSVM and LSVM and $\ell_{\text{support}} = 500$ in MRVM. We did not optimize this hyperparameter.
- **FT3 and FT4:** for FT3 and FT4 we cannot use the *compressive sensing method* and instead solve the following least squares problem

$$\min_{w \in \mathbb{R}^{\ell_3}} \sum_{(x, \hat{v}_i(x)) \in R_i} \left(\hat{v}_i(x) - \underbrace{(F_{\cdot, \mathcal{S}_i}^{-1} w)(x)}_{=\hat{v}_i(x)} \right)^2.$$

In Figure 7, we present a flow diagram of the different algorithms we use in HYBRID ICA.

E.2 Details of NNs Support Discovery Experiments

In this Section, we discuss the energy ratio plot (see Figure 3 in the main paper) for the large domain MRVM with $m = 98$ items. Recall, that in MRVM one cannot compute the full FT analytically and one has to use sparse FT algorithms to obtain an approximation of the true k-best possible frequencies $\mathcal{S}_i^* = \{y^{(1)}, \dots, y^{(k)}\}$. For this we use the recently developed RWHT algorithm from [Amrollahi et al. \(2019\)](#), which computes the largest WHT-FCs with high probability and thus gives us an approximation $\mathcal{S}_i^{\text{rwht}} \approx \mathcal{S}_i^*$. As in the main paper, we then calculate for each bidder $i \in N$ the *energy ratio* of the support found by the corresponding NNs $\hat{\mathcal{S}}_i$ and $\mathcal{S}_i^{\text{rwht}}$.

E.3 Details of Efficiency Experiments

In Figures 8–10, we present detailed efficiency results of HYBRID ICA in all three SATS domains, where we used the best found configuration of hyperparameters from Table 6.

In the upper plot we show in each figure the efficiency of the different phases of HYBRID ICA.⁴ In the lower plot, we present a histogram of the final efficiency distribution over 100 (in GSVM and LSVM) and 30 (in MRVM) new CA instances. To enable a head-to-head comparison, we use for the test set of CA instances the seeds 1–100 in GSVM and LSVM, and seeds 51–80 in MRVM.⁵

⁴In MRVM we abbreviate the different query types as follows: RI=random initial queries, 1-55=MLCA iterations, FR=Fourier reconstruction queries, FA=Fourier allocation queries.

⁵All experiments were conducted on machines with Intel Xeon E5- 2650 v4 2.20GHz processors with 48 logical cores and 128GB RAM and Intel E5 v2 2.80GHz processors with 40 logical cores and 128GB RAM.

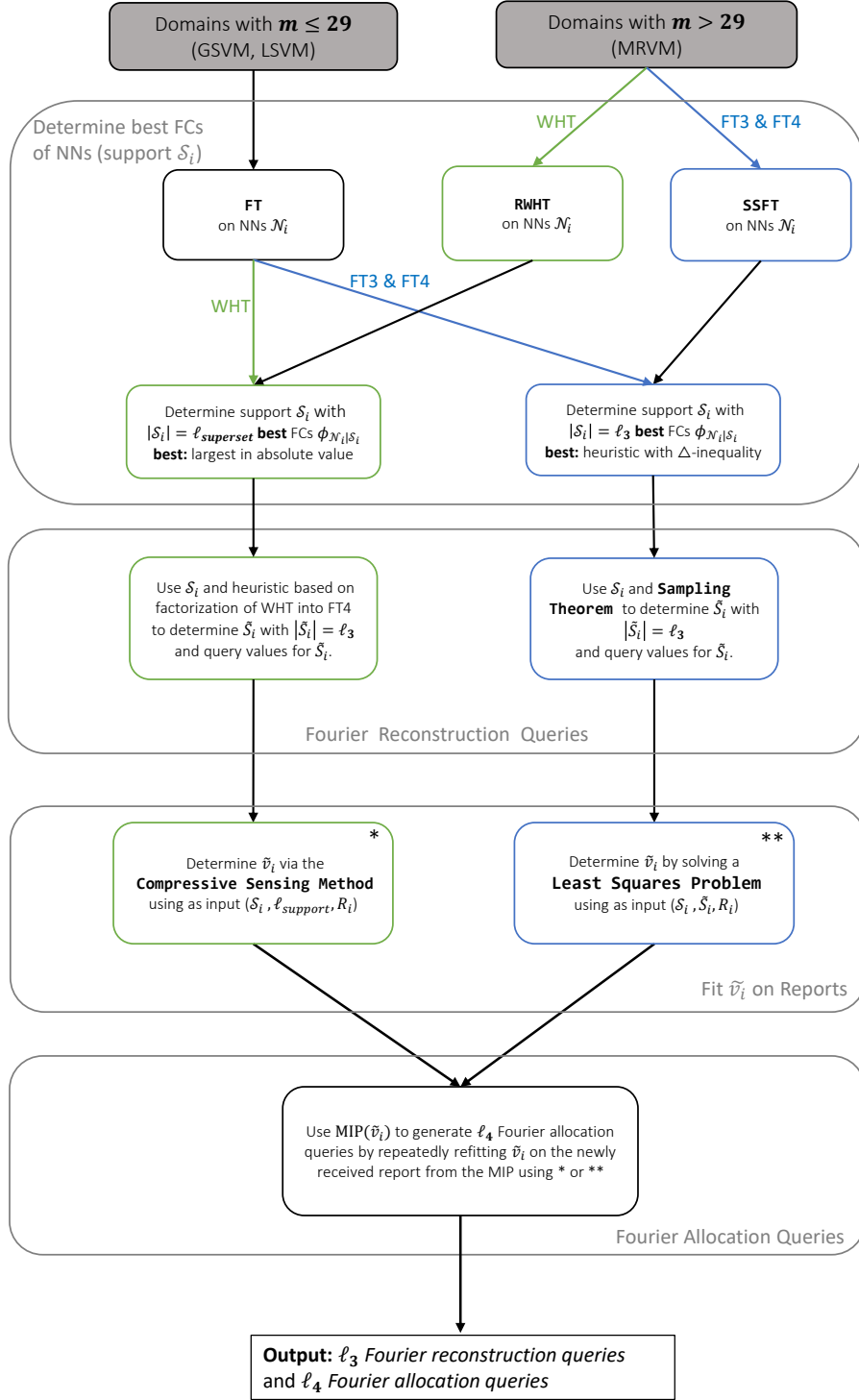
| NNs Architecture | | FT | ℓ_1 | ℓ_2 | ℓ_3 | ℓ_4 |
|------------------|-----------------------------|-----|----------|----------|----------|----------|
| GSVM | R:[32, 32] N:[10, 10] | WHT | 30 | 21 | 20 | 29 |
| LSVM | R:[32, 32] N:[10, 10, 10] | WHT | 30 | 30 | 10 | 30 |
| MRVM | L,R,N:[16, 16] | WHT | 30 | 220 | 0 | 250 |

Table 6: Best configuration of HYBRID ICA.

GSVM (Figure 8) We again reprint the efficiency results of the different paths of HYBRID ICA for GSVM, which is discussed in detail in the main paper. Furthermore, we present in the lower plot a histogram of the final efficiency distribution. We see, that for 94 out of 100 instances HYBRID ICA impressively achieves an economic efficiency of 100% using in total only 100 value queries per bidder.

LSVM (Figure 9) Starting with $\ell_1 = 30$ random initial queries, HYBRID ICA achieves an average efficiency of approximately 62%. Next, HYBRID ICA performs 5 MLCA iterations. After these 5 MLCA iterations, HYBRID ICA already found for each of the 100 instances an allocation with an efficiency of at least 80% with an average efficiency of 97.80%. Here, in the non-sparse LSVM domain, the *Fourier reconstruction and allocation queries* can increase the efficiency of some outliers arriving at an average efficiency of 98.74%. In the histogram, we see, that for 66 instances, HYBRID ICA was able to achieve full efficiency. Overall, we observe, that in the non-sparse LSVM the Fourier-based approach is not as effective as in the sparse GSVM, but still leads to results, that statistically match the efficiency of MLCA (see Table 3 in the main paper).

MRVM (Figure 10) Starting with $\ell_1 = 30$ random initial queries, HYBRID ICA achieves an average efficiency of approximately 50%. Next, HYBRID ICA performs 55 MLCA iterations and asks in total 220 *MLCA allocation queries*. Here, we observe a steep increase in efficiency at the beginning. In later iterations the increase in efficiency gets smaller resulting in an average efficiency of 94.20%. In MRVM, the best query split we found uses $\ell_3 = 0$ Fourier reconstruction queries, thus the Fourier reconstruction queries (FR) do not change the efficiency distribution in Figure 10. However, the $\ell_4 = 250$ *Fourier-based allocation queries* significantly increase the efficiency further by 2.43% resulting in a final average efficiency of 96.63%.



Algorithms:

FT: (Full) Fourier transform, Püschel and Wendler (2020).

RWHT: Robust sparse WHT algorithm, Amrollahi et al. (2019).

SSFT: Sparse set function Fourier transform, Wendler et al. (2020)

Sampling Theorem: Püschel and Wendler (2020).

Compressive Sensing Method: Stobbe and Krause (2012).

Figure 7: Overview of Fourier Transform-based Procedures in HYBRID ICA.

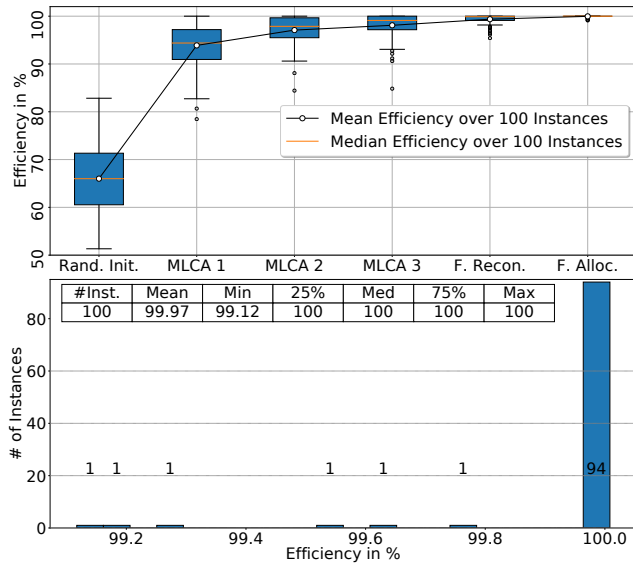


Figure 8: Details of HYBRID ICA in GSVM.

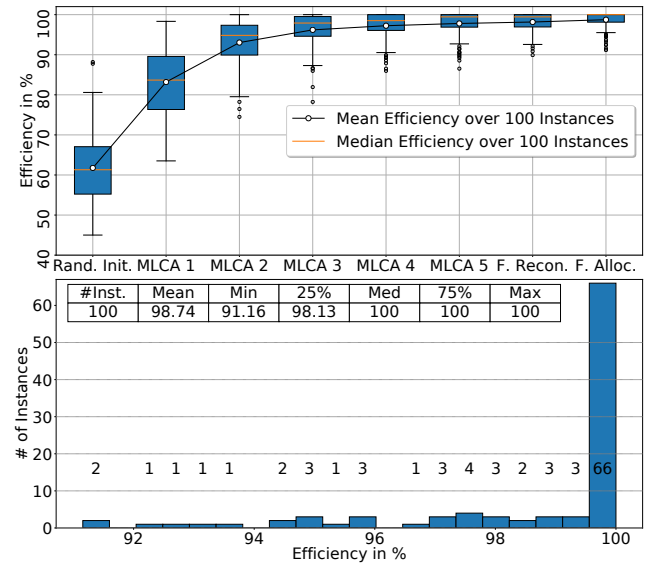


Figure 9: Details of HYBRID ICA in LSVM.

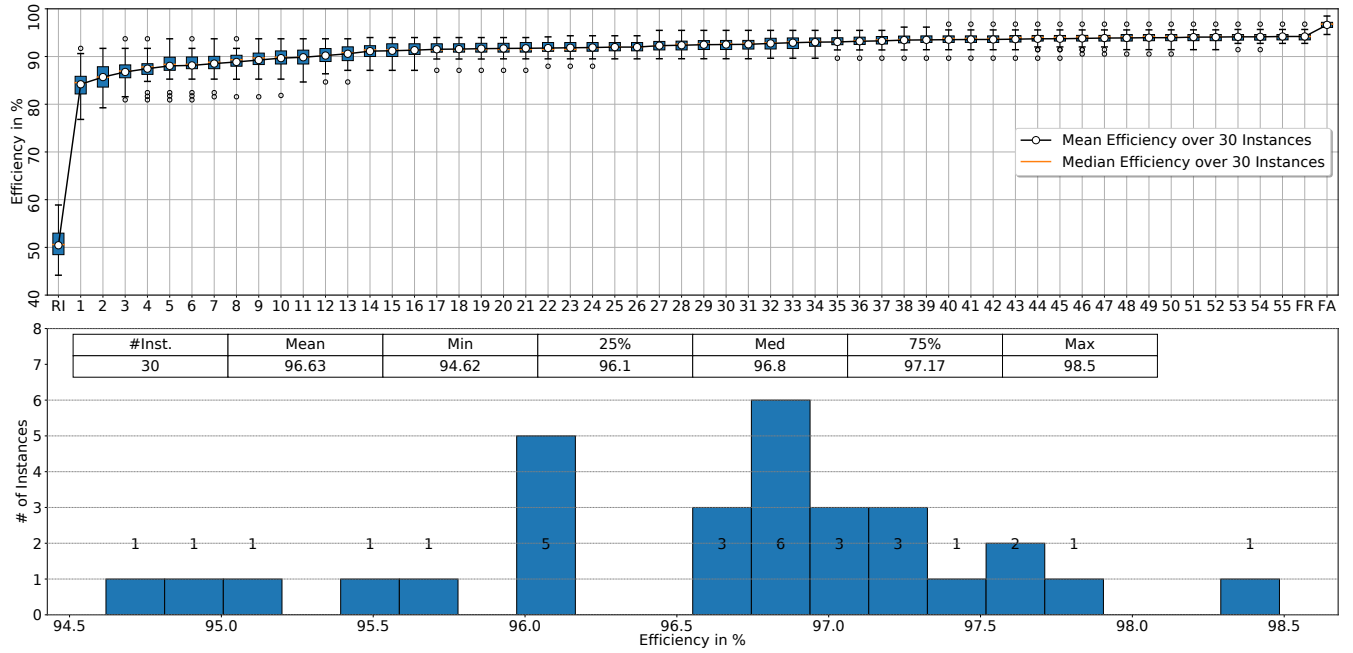


Figure 10: Details of HYBRID ICA in MRVM.